Supplementary Information

Table of Contents

Supplementary Note 1: Examination of experimental parameters for AMC production.

Experimental parameters for each reaction step (surface oxidation, grafting of APTMS, PEGylation) were examined to validate the efficacy of the process.

1) Surface oxidation. Surface oxidation of silane ($Si\text{-}CH_3$) groups in PDMS forms silanol (Si-OH) moieties(1–3), which can react with the trimethoxy groups in APTMS. We compared two methods of surface oxidation: solution phase oxidation by continuous circulation of H_2O/30% (v/v) H_2O_2/12M HCl (in a volume ratio of 5:1:1) (2) through conduits for one hour, and exposure to air plasma(3) for two minutes (plasma oxidation). Oxidized conduits were reacted with APTMS, and the presence of the resulting surface amines was quantitated by labeling with NHS fluorescein and measuring surface fluorescence (Figure S1.1A). Fluorescence was strongest for conduits subjected to plasma oxidation.

After oxidation, surface rearrangements (known as hydrophobic regeneration) can bring un-cross-linked PDMS silane oligomers to the surface, diminishing the proportion of reactive silanol species. This process can be mitigated by extracting PDMS oligomers with organic solvents prior to oxidation(1). PDMS conduits were immersed in hexane for 24 hours prior to acid or plasma oxidation, followed by amino-silanization and fluorescent labeling (Figure S1.1A). PDMS extraction did not influence fluorescence for plasma-oxidized conduits, but decreased the fluorescence after solution phase oxidation. Consequently, solvent extraction was not adapted into the AMC production process.

2) Grafting of APTMS. APTMS (5%, 50% or 100% (v/v) APTMS in acetone) was reacted with plasma-oxidized PDMS conduits for 60 minutes to coat the surfaces with covalently bound primary amine groups (4) (Figure S1.1B), or with 100% (v/v) APTMS for shorter periods. Surface amines from APTMS deposition were labeled with NHS fluorescein and surface fluorescence was measured. Surface fluorescence was similar for all reaction conditions, suggesting similar degrees of modification with APTMS. Consequently, we used 5% (v/v) APTMS in acetone (incubated for 60 minutes) in subsequent experiments to minimize reagent consumption.

3) PEGylation. The amine moieties on the APTMS-modified surfaces were derivatized with NHS-PEG_{10}-MAL, forming PEG spacers on the surface that terminated in maleimide moieties, to which antibodies could be conjugated. Since the reaction of amines with NHS ester is pH dependent(5), the PEGylation reaction was conducted in MES buffer with at pH 7.5, 8.5, and 9.5, and the degree of modification was assessed with

SAMSA fluorescein, which binds to maleimide moieties and results in fluorescent labeling (Figure S1.1C). Surface fluorescence was greatest at pH 8.5 (although the difference was not statistically significant), so subsequent AMC PEGylation was conducted at that pH.

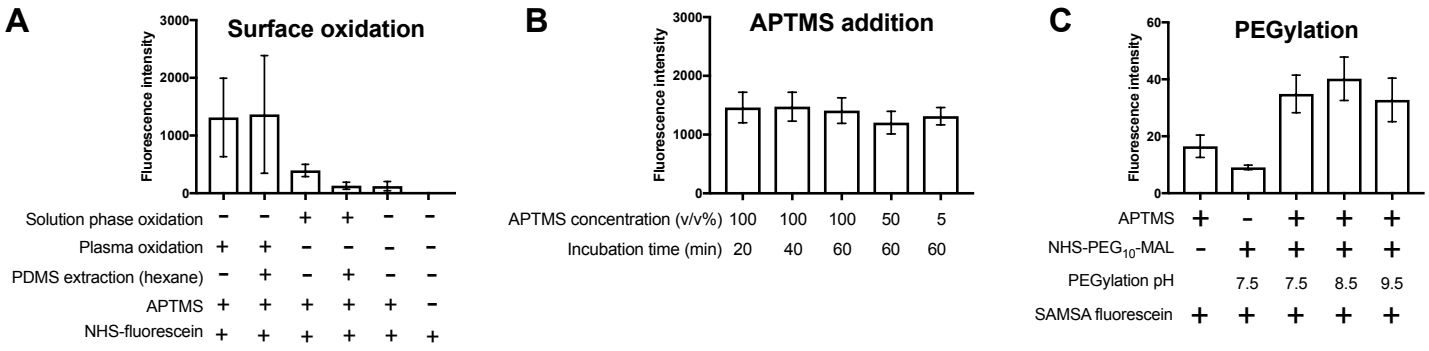

Figure S1.1. Effect of process parameters on surface modification. (A) Effect of solution phase vs. plasma oxidation and of PDMS extraction with hexane on modification with APTMS. (B) Effect of APTMS concentration and reaction duration on modification with APTMS. (C) Effect of reaction pH on PEGylation. Data are means ± SD. n = 4 for each experiment. PDMS: polydimethylsiloxane. APTMS: 3-Aminopropyl)trimethoxy-silane. NHS: *N*-hydroxysuccinimide. NHS-PEG_{10}-MAL: 10 kDa Poly(ethylene glycol) with NHS and maleimide moieties. SAMSA fluorescein: 5-((2-(and-3)-S-(acetylmercapto) succinoyl) amino) fluorescein.

Figure S1.2: rhTNFA elimination by anti-hTNFA conduits.

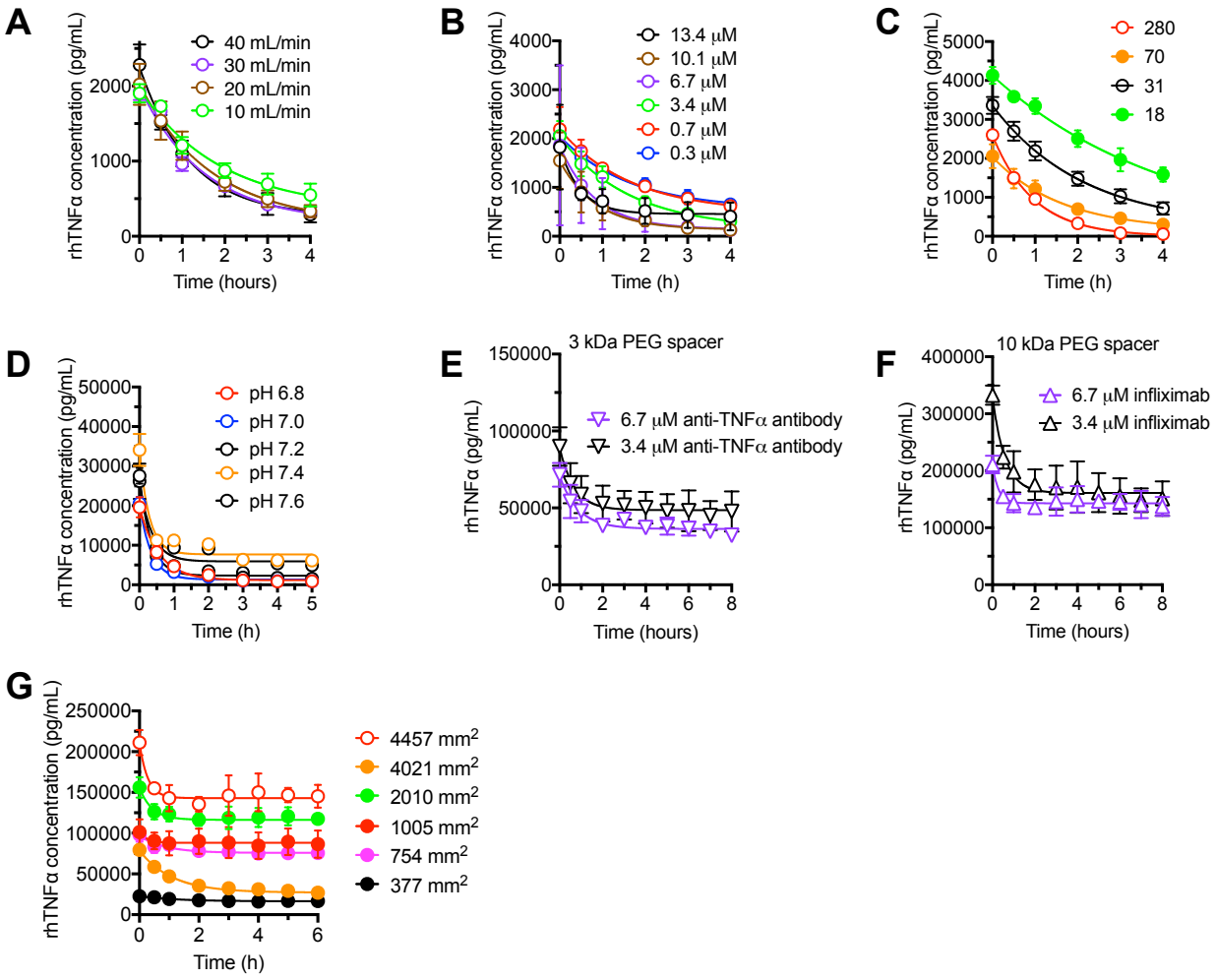

Figure S1.2. Effect of fluid characteristics and AMC properties on the time course of recombinant human TNFA (rhTNFA) elimination by anti-human TNFA antibody modified conduits (anti-hTNFA AMCs): (A) flow rate through AMCs (n = 5 for 10 mL/min, n = 4 for 20 and 30 mL/min, n = 6 for 40 mL/min), (B) concentration of anti-hTNFA antibody used during conjugation (n = 4), (C) AMC aspect ratio (constant surface area)(n = 4), (D) pH of circulating fluid (n = 4), (E,F) poly(ethylene glycol)(PEG) molecular weight and antibody concentration (n = 8 for AMCs prepared with 10 kDa PEG/3.4 μM antibody; n = 4 for all other groups), and (G) AMC surface area (n = 4). All experiments were done in 5% (w/v) BSA. Data are means ± SD. Experimental conditions are shown in supplemental tables S1 – S5.

Supplementary note 2: Unreacted functional groups responsible for non-specific binding.

To assess the possibility that unreacted functional groups in the AMCs were responsible for non-specific binding, PEGylated PDMS conduits (prior to surface antibody conjugation) were treated with molar excesses of mercaptoethanol (200 mM in PBS) to passivate maleimide moieties(6) or acetic anhydride (200 mM in methanol) to passivate (acylate) residual amines(7) on APTMS (supplementary Figure S2A). Solutions of rhVEGF A were circulated through the resulting PEGylated, passivated, antibody-free conduits and elimination of circulating rhVEGF A was assessed. Treatment with acetic anhydride completely prevented elimination of rhVEGF A by PEGylated conduits whereas mercaptoethanol only partially prevented elimination (supplementary Figure S2B), suggesting that residual amine moieties on APTMS were responsible for non-specific binding. All subsequent AMCs were treated with acetic anhydride prior to antibody conjugation (Figure 1B), which completely eliminated non-specific binding of non-targeted cytokines (Figure S2B).

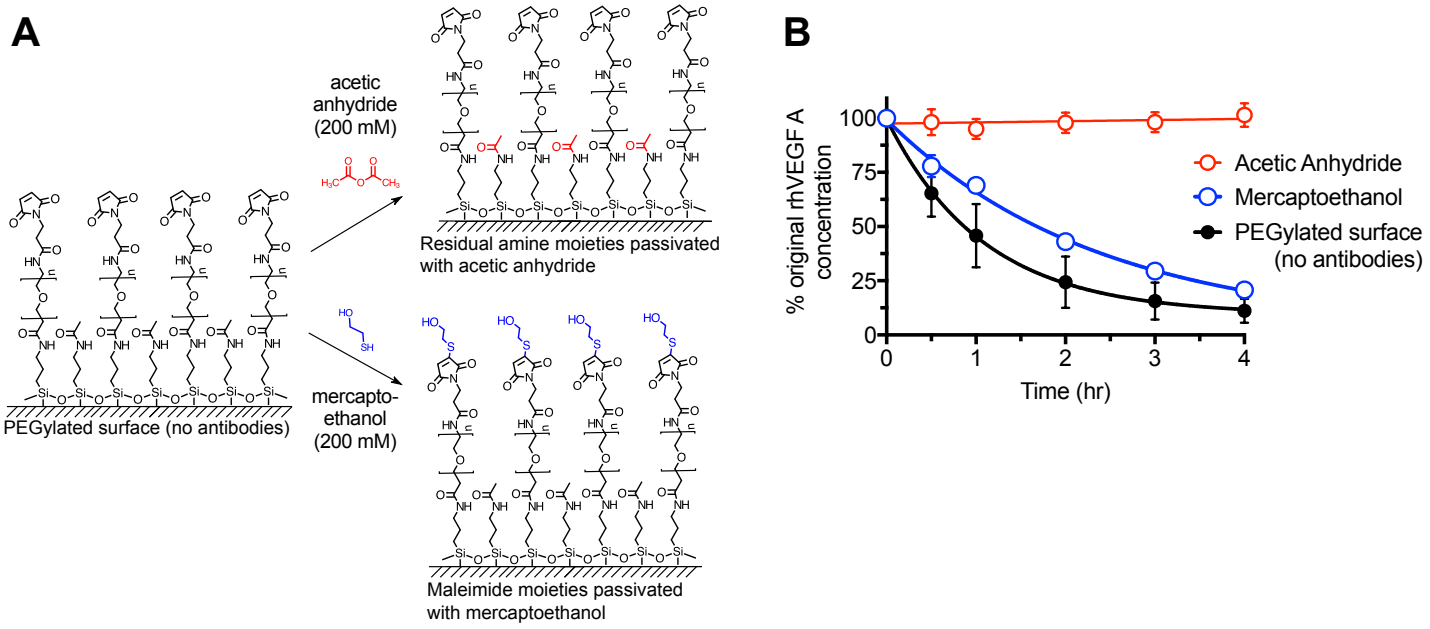

Figure S2. Identification of unreacted functional groups responsible for non-specific binding. (A) Schematic of potential mechanisms of non-specific binding, and of its mitigation with mercaptoethanol or acetic anhydride. (B) Elimination of recombinant vascular endothelial growth factor A (rhVEGF A) via non-specific binding by PEGylated conduits [depicted in panel A] lacking surface antibodies, treated with either mercaptoethanol or acetic anhydride. Cytokine measurements were fitted with one-phase exponential decay curves. All data are means ± SD. n = 4. All cytokine solutions were in 5% (w/v) BSA and circulated at 40 mL/min.

Supplementary Note 3: Effect of circuit acylation on specific binding.

Residual, unreacted amines were responsible for non-specific binding, which was mitigated by acylation with acetic anhydride (main text Figure 3, Supplementary Note 2, figure S3). To assess the effect of pretreatment on AMC function, anti-hTNFA or anti-hVEGF A antibodies were conjugated to PEGylated conduits with or without acylation. Solutions of rhTNFA or rhVEGF A in 5% (w/v) BSA were circulated through the resulting AMCs with starting concentrations as follows: 1,600 ± 210 pg/mL rhVEGF A for acylated anti-hVEGF A AMCs; 1,800 ± 130 pg/mL rhVEGF A for acylated anti-hTNFA AMCs; 2,100 ± 300 pg/mL rhTNFA for acylated anti-hTNFA AMCs; 1,600 ± 220 rhTNFA for acylated anti-hVEGF A AMCs; 2,600 ± 600 pg/mL rhVEGF for non-acylated anti-hVEGF A AMCs; 2,300 ± 100 pg/mL for non-acylated anti-hTNFA AMCs. When cytokines were circulated through acylated AMCs with antibodies against them, they were cleared (Figure S3). However, clearance of rhVEGF A was reduced compared to that by non-acylated AMCs. When cytokines were circulated through AMCs with antibodies to other cytokines, there was no cytokine clearance, i.e. there was no detectable non-specific elimination.

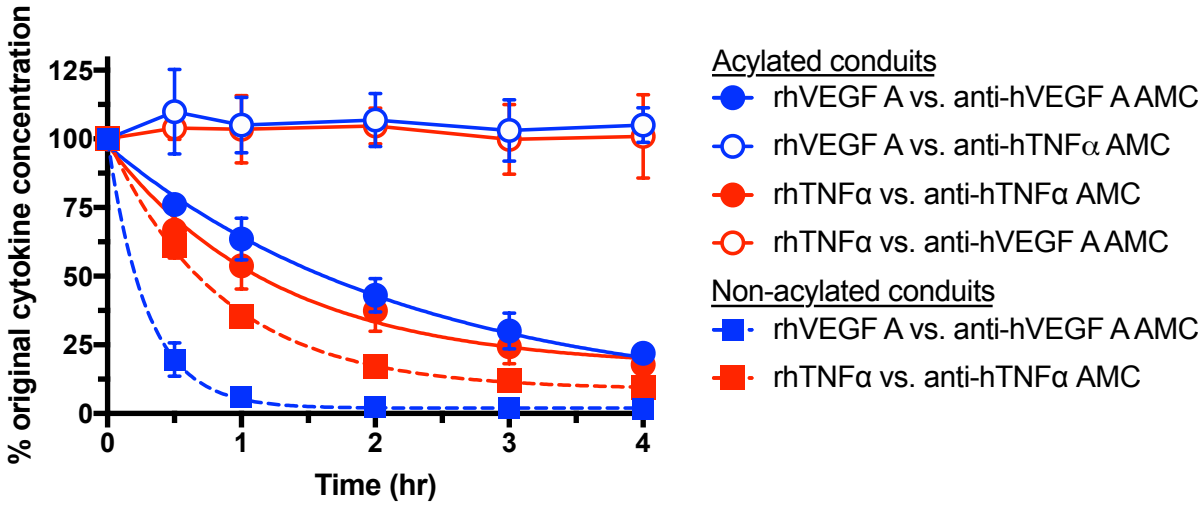

Figure S3. Effect of acylation of antibody modified conduits (AMC) with acetic anhydride (to eliminate non-specific binding) on specific binding. Circulation of recombinant human TNF alpha (rhTNFA) and vascular endothelial growth factor A (rhVEGF A) through anti-human TNF alpha (anti-hTNFA) or anti-human VEGF A (anti-hVEGF A) AMCs with or without acylation prior to antibody conjugation; cytokine measurements were fitted with one-phase exponential decay curves. All data are means ± SD. All cytokine solutions were in 5% (w/v) BSA. Experimental conditions are listed in Table 1 (Condition 1; Flow rate 40 mL/min)(n = 4 for all groups).

Supplementary Note 4: rhTNFA elimination by AMCs from 5% (w/v) BSA vs. human whole blood.

We compared rhTNFA elimination from heparinized human whole blood to elimination from 5% (w/v) BSA in PBS to (1) validate the feasibility of cytokine elimination from blood and (2) determine if 5% (w/v) BSA solutions were suitable surrogates for blood. The $T_{1/2}$ in blood and 5%(w/v) BSA were similar ($p = 0.55$, unpaired, two tailed Student's t-test).

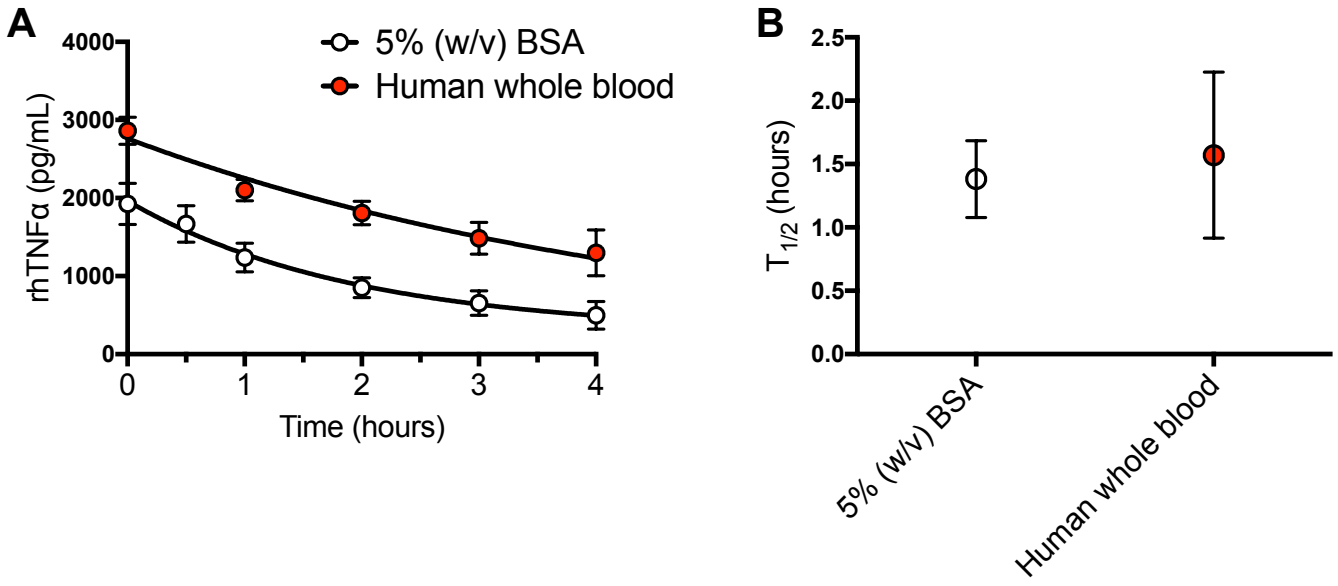

Figure S4. Comparison of recombinant human TNFA (rhTNFA) elimination by anti-human TNFA antibody modified conduits (anti-hTNFA AMC) from 5% (w/v) bovine serum albumin (BSA) or human whole blood. (A) Time course of rhTNFA elimination from solutions of 5% (w/v) BSA in 1x phosphate buffered saline or human whole blood by AMCs. (B) rhTNFA half-lives ($T_{1/2}$) derived from elimination curves in (A). Experimental conditions are listed in Table 1 (Condition 2). All data are means ± SD. n = 4 for each group.

Supplementary Tables S1 – S5: Variables that determine AMC performance.

Table S1. The effect of flow rate through anti-hTNFA AMCs on rhTNFA elimination half-life ($T_{1/2}$). Also shown is the characterization of anti-hVEGF A AMCs constructed with the same design parameters (i.e. a different antibody).

Variable studied	Surface antibody	Length (mm)	I.D. (mm)	Aspect ratio	S.A. (mm^2)	PEG MW (kDa)	Ab. conc. (μM)	Flow rate (mL/min)	Circulating pH	$T_{1/2}$ (hr)	Capacity (ng)	n
Flow rate through AMCs	anti-hTNFA	222	3.2	70	2251	10	3.4	10	7.4	1.4 ± 0.4	--	5
	anti-hTNFA	222	3.2	70	2251	10	3.4	20	7.4	1.5 ± 0.2	--	4
	anti-hTNFA	222	3.2	70	2251	10	3.4	30	7.4	1.0 ± 0.2	--	4
	anti-hTNFA	222	3.2	70	2251	10	3.4	40	7.4	0.8 ± 0.1	--	6
Different antibody	anti-hVEGF A	222	3.2	70	2251	10	3.4	40	7.4	1.4 ± 0.3	--	4

TNFA (tissue necrosis factor alpha)
I.D. (inner diameter)
Aspect ratio (AMC length / inner diameter)
Ab. Conc. (antibody concentration)
S.A. (surface area)
PEG MW (poly(ethylene glycol) molecular weight)
AMC (antibody modified conduit)
anti-hTNFA (anti-human tissue necrosis factor alpha)
anti-hVEGF A (anti-human vascular endothelial growth factor A)

Table S2. The effect of anti-hTNFA antibody concentration on rhTNFA elimination half-life ($T_{1/2}$).

Variable studied	Surface antibody	Length (mm)	I.D. (mm)	Aspect ratio	S.A. (mm^2)	PEG MW (kDa)	Ab conc. (μM)	Flow rate (mL/min)	pH	$T_{1/2}$ (hr)	Capacity (ng)	n
Ab. conc. during AMC synthesis	anti-hTNFA	222	3.2	70	2251	10	0.3	20	7.4	2.6 ± 0.6	--	4
	anti-hTNFA	222	3.2	70	2251	10	0.7	20	7.4	2.3 ± 0.3	--	4
	anti-hTNFA	222	3.2	70	2251	10	0.3	20	7.4	1.5 ± 0.2	--	4
	anti-hTNFA	222	3.2	70	2251	10	0.7	20	7.4	0.8 ± 0.1	--	4
	anti-hTNFA	222	3.2	70	2251	10	6.7	20	7.4	0.7 ± 0.1	--	4
	anti-hTNFA	222	3.2	70	2251	10	10.1	20	7.4	0.8 ± 0.1	--	4

TNFA (tissue necrosis factor alpha)
I.D. (inner diameter)
Aspect ratio (AMC length / inner diameter)
Ab. conc. (antibody concentration)
S.A. (surface area)
PEG MW (poly(ethylene glycol) molecular weight)
AMC (antibody modified conduit)
anti-hTNFA (anti-human tissue necrosis factor alpha)

Table S3. The relationship between anti-hTNFA AMC aspect ratio and rhTNFA elimination half-life ($T_{1/2}$)

Variable studied	Surface antibody	Length (mm)	I.D. (mm)	Aspect ratio	S.A. (mm^2)	PEG MW (kDa)	Ab conc. (μM)	Flow rate (mL/min)	pH	$T_{1/2}$ (hr)	Capacity (ng)	n
AMC geometry (aspect ratio)	anti-hTNFA	445	1.6	280	2217	10	3.4	20	7.4	0.7 ± 0.03	--	4
	anti-hTNFA	222	3.2	70	2217	10	3.4	20	7.4	1.1 ± 0.1	--	4
	anti-hTNFA	148	4.8	31	2217	10	3.4	20	7.4	1.5 ± 0.2	--	4
	anti-hTNFA	111	6.4	18	2217	10	3.4	20	7.4	2.2 ± 0.5	--	4

TNFA (tissue necrosis factor alpha)
I.D. (inner diameter)
Aspect ratio (AMC length / inner diameter)
Ab. conc. (antibody concentration)
S.A. (surface area)
PEG MW (poly(ethylene glycol) molecular weight)
AMC (antibody modified conduit)
anti-hTNFA (anti-human tissue necrosis factor alpha)

Table S4. The effect of circulating pH on rhTNFA elimination half-life ($T_{1/2}$)

Variable studied	Surface antibody	Length (mm)	I.D. (mm)	Aspect ratio	S.A. (mm^2)	PEG MW (kDa)	Ab conc. (μM)	Flow rate (mL/min)	pH	$T_{1/2}$ (hr)	Capacity (ng)	n
pH of circulating fluid	anti-hTNFA	886	1.6	554	4458	10	3.4	20	6.8	0.4 ± 0.09	--	4
	anti-hTNFA	886	1.6	554	4458	10	3.4	20	7.0	0.2 ± 0.03	--	4
	anti-hTNFA	886	1.6	554	4458	10	3.4	20	7.2	0.2 ± 0.05	--	4
	anti-hTNFA	886	1.6	554	4458	10	3.4	20	7.4	0.2 ± 0.08	--	4

TNFA (tissue necrosis factor alpha)
I.D. (inner diameter)
Aspect ratio (AMC length / inner diameter)
Ab. conc. (antibody concentration)
S.A. (surface area)
PEG MW (poly(ethylene glycol) molecular weight)
AMC (antibody modified conduit)
anti-hTNFA (anti-human tissue necrosis factor alpha)

Table S5. Augmentation of rhTNFA half-life ($T_{1/2}$) and AMC capacity (total mass of captured rhTNFA) by changing PEG molecular weight or AMC surface area.

Variable studied	Surface antibody	Length (mm)	I.D. (mm)	Aspect ratio	S.A. (mm^2)	PEG MW (kDa)	Ab conc. (μM)	Flow rate (mL/min)	pH	$T_{1/2}$ (hr)	Capacity (ng)	n
PEG MW (and antibody conc.)	anti-hTNFA	886	1.6	554	4458	10	3.4	20	7.4	0.2 ± 0.1	2355 ± 800	4
	anti-hTNFA	886	1.6	554	4458	10	6.7	20	7.4	0.5 ± 0.1	3417 ± 778	4
	anti-hTNFA	886	1.6	554	4458	3	3.4	20	7.4	1.7 ± 0.1	823 ± 84	8
	anti-hTNFA	886	1.6	554	4458	3	6.7	20	7.4	1.8 ± 0.6	869 ± 384	4
AMC surface area	anti-hTNFA	886	1.6	554	4458	10	3.4	20	7.4	0.2 ± 0.1	2355 ± 800	4
	anti-hTNFA	400	3.2	125	4021	10	3.4	20	7.4	0.8 ± 0.2	1026 ± 128	4
	anti-hTNFA	400	1.6	250	2011	10	3.4	20	7.4	0.8 ± 0.2	776 ± 321	4
	anti-hTNFA	150	1.6	94	1005	10	3.4	20	7.4	0.5 ± 0.4	438 ± 213	4
	anti-hTNFA	400	0.8	500	754	10	3.4	20	7.4	0.4 ± 0.3	270 ± 232	4
	anti-hTNFA	150	0.8	188	377	10	3.4	20	7.4	0.7 ± 0.2	118 ± 25	4

TNFA (tissue necrosis factor alpha)
I.D. (inner diameter)
Aspect ratio (AMC length / inner diameter)
Ab. conc. (antibody concentration used during conjugation)
S.A. (surface area)
PEG MW (poly(ethylene glycol) molecular weight)
AMC (antibody modified conduit)
anti-hTNFA (anti-human tissue necrosis factor alpha)

Supplementary Note 5: Cytokine response to lipopolysaccharide injection.

We sought to identify a dose of lipopolysaccharide (LPS) that would result in rapidly elevated cytokine levels after intravenous injection. Rats underwent left femoral vein (RFV) then right femoral artery cannulation under isoflurane/oxygen anesthesia (see Methods). A single intravenous dose of LPS (12.5 – 17.5 mg/kg) was injected into the RFV and rats remained under anesthesia for the next 12 hours or until they died. No extracorporeal circulation was performed in these experiments. Arterial blood (200 μL) was sampled before LPS injection and every two hours thereafter for cytokine measurement (see Methods). The highest dose studied (17.5 mg/kg) yielded elevated cytokine levels within 2 hours, which persisted over the course of experiments (except for TNFA, which decreased rapidly after 2 hours)(Figure S5).

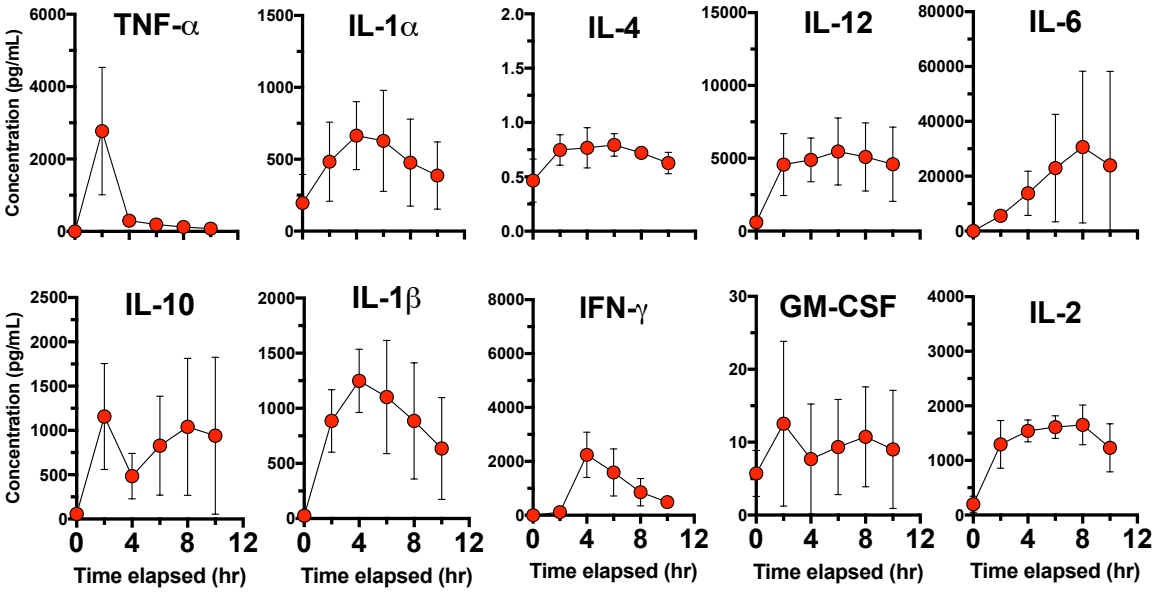

Figure S5. Plasma concentrations (pg/mL) of cytokines in rats following intravenous injection of 17.5 mg/kg lipopolysaccharide (LPS). Data are means ± S.D. (n = 4).

Supplementary Note 6: Area under the curve analysis to determine the total mass of IL-1B detected in plasma during an episode of hypercytokinemia.

We used area under the curve (AUC) analysis to determine the total mass of rIL-1BB expressed in the blood in response to LPS injection over the time course of experiments. Using weight based calculations of circulating blood volume(8), the duration of rIL-1B sampling (denoted as $Time$ in the following equation) and calculated AUC values (from the rIL-1B curves in Figures 5b and S5), it was possible to calculate the total mass of rIL-1B detected in plasma during each experiment with the following equation:

$$Total\ detected\ mass\ of\ r\mathrm{IL}-1\mathrm{B}\ = (AUC\ x\ circulating\ blood\ volume)/Time$$

Total detected mass of rIL-1B was then used to define the minimum capacity that anti-rIL-1B AMCs must possess to ensure complete clearance of rIL-1B from the vascular space. Table S6 shows the calculated result for each parameter. The total detected mass of rIL-1B was 31.1 ± 14.1, which we defined as the minimum benchmark capacity anti-rIL-1B AMCs must possess to be considered for use in vivo.

Table S6. AUC analysis to determine total mass of rIL-1β detected in the plasma of rats following injection of intravenous lipopolysaccharide (n = 4).

Parameter	Result
AUC (pg x hr/mL)	8.6 ± 3.6
Blood volume[1] (mL)	33.9 ± 4.0
Time[2] (hr)	9.5 ± 1.0
Total detected mass of IL-1β[3] (pg)	31.1 ± 14.1

Data are presented as means ± SD of n observations
rIL-1β (rat interleukin 1 beta)
AUC (area under the curve for measured blood levels of IL-1β)
[1]Blood volume (mL) = (0.06 x BW) + 0.77, where BW = body weight (from reference 8)
[2]Time point of last cytokine measurement
[3]Total mass of IL-1β measured in plasma over course of experiment = (AUC x blood volume) / Time

Supplementary Note 7: Area under the curve analysis comparing total detected mass of IL-1B between treatment groups.

We hypothesized that the total mass of rIL-1B eliminated by anti-rIL-1B AMCs was equal to the difference between the total detected mass of rIL-1B in rats treated with anti-hVEGF A AMCs and rats treated with anti-rIL-1B AMCs. Using weight-based calculations of circulating blood volume(8), durations of rIL-1B sampling and calculated AUC values, we determined the total mass of rIL-1B detected in plasma for each experimental group (Table S7). Rats treated with anti-rIL-1B AMCs yielded 0.4 ± 0.2 ng of rIL-1B compared to 6.4 ± 4.5 ng for animals treated with anti-hVEGF A AMCs ($p = 0.009$, unpaired t test). The total mass of rIL-1B eliminated by anti-rIL-1B AMCs was then determined by calculating the difference in total detected rIL-1B mass between the two experimental groups [6.0 ± 4.3, which was approximately 15.6 % of total AMC capacity for the anti-rIL-1B AMCs used in this study].

Table S7. AUC analysis to determine total mass of rIL-1B detected in the plasma of rats treated with anti-rIL-1B or anti-hVEGF A AMCs.

Parameter	anti-rIL-1B AMC (n = 6)	anti-hVEGF A AMC (n = 4)	P value
AUC (ng x hr/mL)	0.1 ± 0.02	3.1 ± 2.4	0.01*
Blood volume[1] (mL)	31.7 ± 4.6	26.5 ± 1.1	0.06
Time[2] (hr)	9.3 ± 2.9	12.3 ± 1.0	0.08
Total detected mass of IL-1β[3] (pg)	0.4 ± 0.2	6.9 ± 5.7	0.01*

Data are presented as means ± SD of n observations
rIL-1B (rat interleukin 1 beta)
AUC (area under the curve for measured blood levels of IL-1β)
[1]Blood volume (mL) = (0.06 x BW) + 0.77, where BW = body weight (from reference 8)
[2]Time point of last cytokine measurement
[3]Total mass of IL-1β measured in plasma over course of experiment = (AUC x blood volume) / Time
* P value < 0.05 denotes statistical significance; Unpaired, two tailed Student's t-test

Figure S6: Biochemical, hemodynamic and survival data from in vivo experiments.

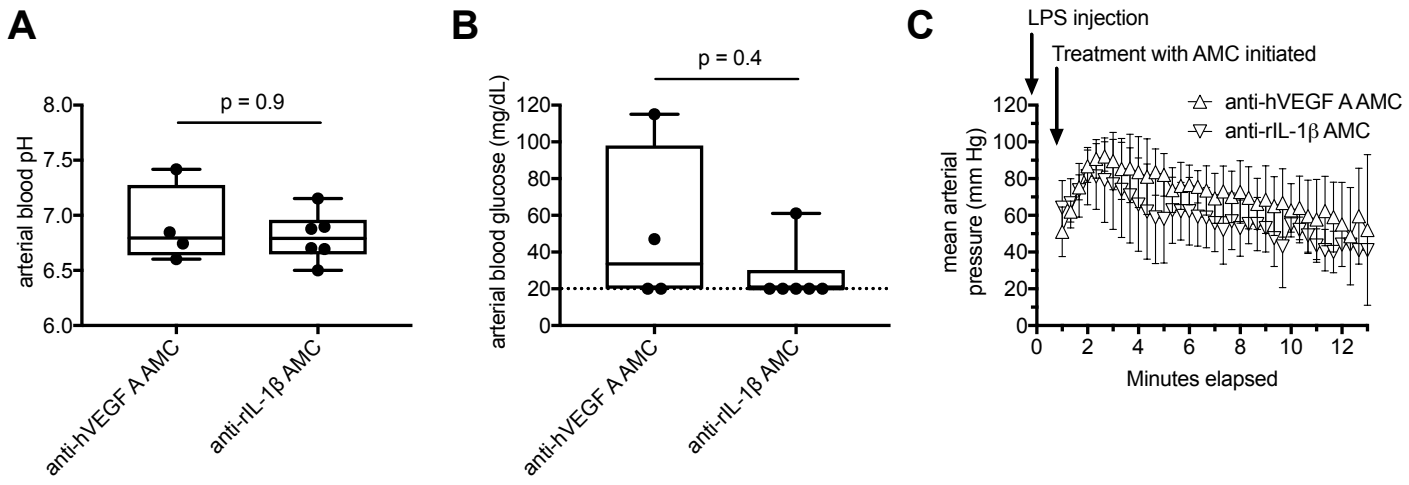

Figure S6. Biochemical and hemodynamic parameters for rats injected with lipopolysaccharide (LPS) and then treated with either anti-human vascular endothelial growth factor A or anti-rat interleukin one beta antibody modified conduits (anti-hVEGF A and anti-rIL-1β AMCs respectively): (A) Arterial blood pH, (B) arterial blood glucose (lowest limit of detection 20 mg/dL, indicated by dotted line), (C) mean arterial pressure ± S.D. For (A) and (B) data are presented as median ± interquartile range (box plots) with min and max values (whiskers); comparisons were made using the Mann-Whitney U test.

Supplementary Note 8: Simultaneous elimination of two different cytokines using AMCs endowed with two antibodies.

We sought to demonstrate that AMCs could eliminate two cytokines simultaneously. To accomplish this, AMCs were prepared by simultaneously introducing 1.7μM anti-hVEGF A antibody and 1.7 μM anti-hTNFA antibody to maleimide-PEG-modified conduits. Solutions of rhVEGF A and rhTNFA in 5% (w/v) BSA were circulated through the resulting anti-hTNFA/anti-hVEGF A AMCs and elimination of circulating rhVEGF A rhTNFA was assessed (Figure S7) to determine $T_{1/2}$ values (Table S8). Both cytokines were simultaneously eliminated.

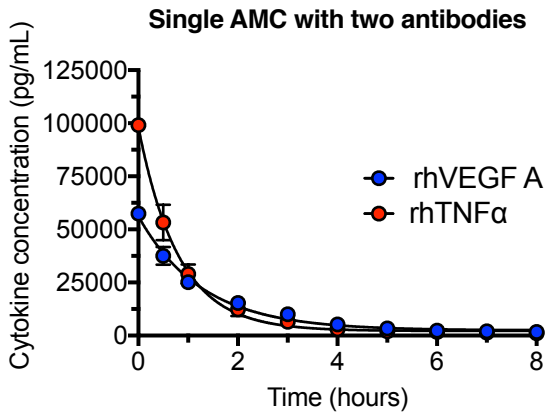

Figure S7. Simultaneous elimination of recombinant human tissue necrosis factor alpha (rhTNFA) and vascular endothelial growth factor A (rhVEGF A) from 5% (w/v) bovine serum albumin in phosphate buffered saline using antibody modified conduits (AMC) endowed with two antibodies: anti-hVEGF A and anti-hTNFA. Experimental conditions are shown in Table S8. Data are means ± S.D. (n = 4).

Table S8. Characteristics of anti-hTNFA + anti-hVEGF A AMCs (i.e. AMCs endowed with two different antibodies).

Variable studied	Surface antibody	Target cytokine(s)	Length (mm)	I.D. (mm)	Aspect ratio	S.A. (mm^2)	PEG MW (kDa)	Ab. conc (μM)	Flow rate (mL/min)	pH	$T_{1/2}$ (hr)	n
Two antibodies	anti-hTNFA and anti-hVEGF A	rhTNFA and rhVEGF A	886	1.6	554	4458	10	1.7	20	7.4	0.6 ± 0.1 (rhTNFA) and 0.9 ± 0.1 (rhVEGF A)	4

rhTNFA (recombinant human tissue necrosis factor alpha)
rhVEGF A (recombinant human vascular endothelial growth factor A)
I.D. (inner diameter)
Aspect ratio (AMC length / inner diameter)
Ab. conc. (antibody concentration)
S.A. (surface area)
PEG MW (poly(ethylene glycol) molecular weight)
anti-hTNFA (anti-human tissue necrosis factor alpha)
anti-hVEGF A (anti-human vascular endothelial growth factor A)

Supplementary Note 9: Detailed derivation of descriptive model.

We developed a theoretical model to describe AMC performance. Cytokine elimination from circulating fluid occurs when cytokines in the fluid bind to surface antibodies and is described by the Langmuir adsorption isotherm. The fraction of antibodies with bound cytokines (θ) depends on the concentration of cytokines at the conduit surface (c_s) and the affinity of surface antibodies for those cytokines (dissociation constant, K_d) according to the following relation(9):

$$\theta = \frac{1}{1 + K_d/c_s}$$

Effective cytokine elimination (large θ) occurs when the antibody affinity for a given cytokine is high (small K_d) and the initial concentration of that cytokine (c_0) significantly exceeds K_d. Otherwise most of the antibodies will remain un-bound (small θ). A second necessary condition for large θ is that the quantity of surface antibodies must be greater than or equal to the quantity of cytokine molecules in the solution. Under these conditions, nearly complete clearance of the cytokine is expected (Figure S8A, case A). If the affinity is high, but the number of antibodies is less than the number of cytokine molecules (either from low surface antibody packing density or insufficient AMC surface area with optimal antibody packing density), then the cytokine concentration will decay until AMC capacity is saturated (Figure S8A, case B). Experimental data showed both patterns, where the cytokine concentration either decreased to zero (Figure S1.2A,B,C) or a steady value (Figures 5C and S1.2D,E,F,G). In the latter case, the amount of unbound cytokine remaining in circulation is given by $M = M_0 - C$, where M_0 is the initial amount of cytokine in the reservoir and C is AMC capacity. Provided $c_0 \gg K_d$, then the number of antibodies available for binding is a good approximation of capacity. AMC capacity did not increase (Figure 4F) over the antibody concentration range that yielded the most rapid cytokine elimination (Figure 4B,E), suggesting that AMC capacity in those experiments was limited by surface area. Consequently, further increases in capacity could only be attained by increasing AMC surface area (Figure 4H).

Cytokine uptake by antibodies involves two main steps: transport of cytokine to surface antibodies and subsequent binding. The flow of cytokine containing fluid through the AMC is accompanied by the formation of boundary layers, which are regions close to the wall where, there exists a concentration and velocity gradient

(Figure S8B). The concentration boundary layer is formed because of the presence of antibodies, which reduce the cytokine concentration near the surface to zero establishing a concentration gradient across the cross section of the AMC. The thickness of this boundary layer (δ_c) depends on diffusivity ($\mathcal{D}$), or the ability of the cytokine to diffuse from the bulk solution to the wall where it can interact with the antibodies. The velocity boundary layer arises because the fluid in contact with the wall has zero velocity in comparison to the bulk fluid, which is being circulated at a certain flow rate. The velocity gradient arises because of viscosity, or relative motion between fluid molecules and gives rise to shear in the fluid. The thickness of this boundary (δ_v) layer depends on fluid viscosity. Both, the velocity and concentration boundary layers vary in their thickness up to a certain length, referred to as the hydrodynamic entrance length (L_H) and concentration entrance length (L_C) respectively, beyond which their thickness is constant and the velocity/concentration profile across the length remains unchanged (Figure S8B). If the length of the AMC is much more than the entrance length, the flow is referred to as developed. Depending upon the flow parameters, tube geometry and diffusivity of the species involved in mass transport, the flow may or may not be developed velocity-wise, concentration-wise or both.

If the antibody affinity is high and antibodies are available for binding, uptake of cytokine by the antibody depletes cytokine within the concentration boundary layer near the wall, the thickness of which is governed by the combination of laminar flow in the axial direction and cytokine diffusion in the radial direction. The time scale for diffusion across the concentration boundary layer to the AMC wall where binding takes place can be estimated to be $\delta^2/\mathcal{D}$ based on Fick's law of diffusion. For binding to occur between the antibody and cytokine, the diffusion time scale must be at least equal to (if not shorter than) the time scale for fluid flow from one end of the AMC to the other, as otherwise, the cytokine will cross the AMC without interacting with the antibody-coated surface. The time scale for fluid flow can be estimated to be L/V, where V is the fluid velocity, and L is the AMC length. Equating the two time scales gives Equation 1.

Equation 1

$$\delta^2 \approx \frac{\mathcal{D}L}{V}$$

Further, in fully-developed pressure driven laminar flows, it can be assumed that the velocity within the boundary layer scales linearly with the distance from the wall (Equation 2). For the conditions under which the experiments were conducted, the velocity profile was predicted to be fully developed, except in a very few cases and the flow was found to be laminar (based on Reynolds Number calculations). This approximation is valid as long as the ratio of the concentration boundary layer thickness to the AMC diameter is much smaller than 1, which for all experimental conditions tested was of the order of 10^{-2}.

Equation 2

$$V \sim \gamma\delta$$

Here, V is the fluid velocity within the boundary layer and γ is the fluid shear at the wall. Equation 1 and 2 were then combined to give an expression for the concentration boundary layer thickness (Equation 3)

Equation 3

$$\delta \sim \sqrt[3]{\frac{\mathcal{D}L}{\gamma}}$$

As the fluid velocity varies roughly between zero to the average flow velocity, U_0 (which can be expressed in terms of the volume flow rate $\dot{\forall}$ and AMC diameter D), an order of magnitude of estimate for γ can be obtained using Equation 4.

Equation 4

$$\gamma \sim \frac{U_0}{D} \sim \frac{\dot{\forall}}{\pi D^3}$$

Combining Equation 3 and 4, an expression for δ can be obtained in terms of all known parameters (Equation 5).

Equation 5

$$\delta \sim \sqrt[3]{\frac{\pi D^3 \mathcal{D} L}{\dot{\forall}}}$$

As described in in the main text, the elimination of cytokines will be limited to an annular region near the AMC surface having a thickness of δ. The mass clearance rate of cytokines can therefore be expressed as shown in Equation 6, where A is the area of the annulus, C is the cytokine concentration and V is the velocity.

Equation 6

$$\dot{m} = A\ C\ V = (\pi D \delta)\ C\ V \sim (\pi D \delta)\ C\ \frac{U_0}{D} \delta$$

Substitution of Equation 5 in 6 gives Equation 7.

Equation 7

$$\dot{m} \sim \pi C\ (\frac{\pi D^3 \mathcal{D} L}{4\dot{\forall}})^{2/3}\ U_0 \sim C\ \sqrt[3]{4\pi^2 \mathcal{D}^2 L^2 \dot{\forall}}$$

The rate of change in cytokine concentration, $\dot{C}$ depends on the mass clearance rate $\dot{m}$ and reservoir volume $\forall$, as shown in Equation 8, which in combination with Equation 7 gives Equation 9.

Equation 8

$$\dot{C} = \frac{dC}{dt} = -\frac{\dot{m}}{\forall}$$

Equation 9

$$\frac{dC}{dt} \sim -\frac{C}{\forall}\sqrt[3]{4\pi^2\mathcal{D}^2L^2\dot{\forall}}$$

Equation 9 can be integrated to predict the variation in cytokine concentration in the reservoir over time (Equation 10 and 11), which can be then used to estimate the rate of cytokine removal by the AMC or the cytokine half-life (Equation 12).

Equation 10

$$\frac{dC}{C} \sim -\frac{\sqrt[3]{4\pi^2\mathcal{D}^2L^2\dot{\forall}}}{\forall}\ dt$$

Equation 11

$$C = C_0\ e^{-\frac{t}{\tau}}$$

Equation 12

The rate at which the cytokine concentration is reduced in the reservoir, can be estimated with Equation 13.

Equation 13

$$\tau = \frac{\forall}{\sqrt[3]{4\pi^2\mathcal{D}^2L^2\dot{\forall}}}, \qquad T_{\frac{1}{2}} = 0.693\,\tau = 0.693\,\frac{\forall}{\sqrt[3]{4\pi^2\mathcal{D}^2L^2\dot{\forall}}}$$

The expression used above can be validated with by the solution to a very commonly studied flow and transport problem for laminar fluid flow between two surfaces separated by a constant thickness, referred to as the Lévêque problem(10). The solution applies to a mass transfer problem, where the solute in the incoming fluid reacts with the surface to reach a constant concentration, different from the inflow. For our purpose, the cytokine concentration at the surface could be zero or non-zero depending on whether the antibodies are saturated or not. The Sherwood number (Sh), which, denotes the volumetric clearance rate per unit area, is given by Equation 14. Here, Re denotes the Reynolds number and Pr denotes the Prandtl number. Expressions for Re and Pr have been given in Equation 15, where ρ denotes fluid density and μ denotes fluid viscosity.

Equation 14

$$Sh = 1.615\sqrt[3]{Re\,\mathrm{Pr}\frac{D}{L}}$$

Equation 15

$$Re = \frac{\rho U_0 D}{\mu}, \qquad \mathrm{Pr} = \frac{\mu}{\rho\mathcal{D}}$$

Substitution of Equation 15 in 14 gives the following expression for Sh (Equation 16)

Equation 16

$$Sh = 1.615\sqrt[3]{\frac{D^2U_0}{\mathcal{D}L}} = 1.615\sqrt[3]{\frac{4\dot{\forall}}{\pi\mathcal{D}L}}$$

The total volumetric clearance rate across the entire AMC can then be expressed as shown in Equation 17

Equation 17

$$\dot{\forall}_c = \pi\mathcal{D}LSh = 1.615\sqrt[3]{4\pi^2\mathcal{D}^2L^2\dot{\forall}}$$

It can be seen that Equation 13 and 17 are similar in terms of their dependence on the parameters involved. We note that equations 13 and 17 ($T_{\frac{1}{2}} = 0.693\frac{\forall}{\sqrt[3]{4\pi^2\mathcal{D}^2L^2\dot{\forall}}}$ and $\dot{\forall}_c = 1.615\sqrt[3]{4\pi^2\mathcal{D}^2L^2\dot{\forall}}$ respectively) hold only in the case where the AMC capacity is much greater than the cytokine amount (i.e. $M_0 < C$). If not, the upstream end of the conduit will be saturated with cytokines and effectively shorten the length L of the conduit, slowing cytokine clearance).

The rate of change in cytokine concentration predicted by the model (Equation 13) correlated linearly (R^2 value = 0.8) to that obtained by fitting exponential curves to the data (Figure S8C). The model also predicted volumetric clearance (i.e. the volume of solution from which the target cytokine is completely eliminated per unit time; m^3/s). Predicted volumetric clearance (Equation 17) correlated linearly with measured values (R^2 value = 0.9; Figure S8D). (The measured volumetric clearance ($\dot{\forall}_c$) was obtained by dividing the fluid volume in the reservoir ($\forall$) by the time constant τ). Thus, the theoretical model accurately describes (and quantifies) AMC function, and can be used to predict, cytokine half-life and the volume of blood a given AMC will clear based on input parameters for that AMC.

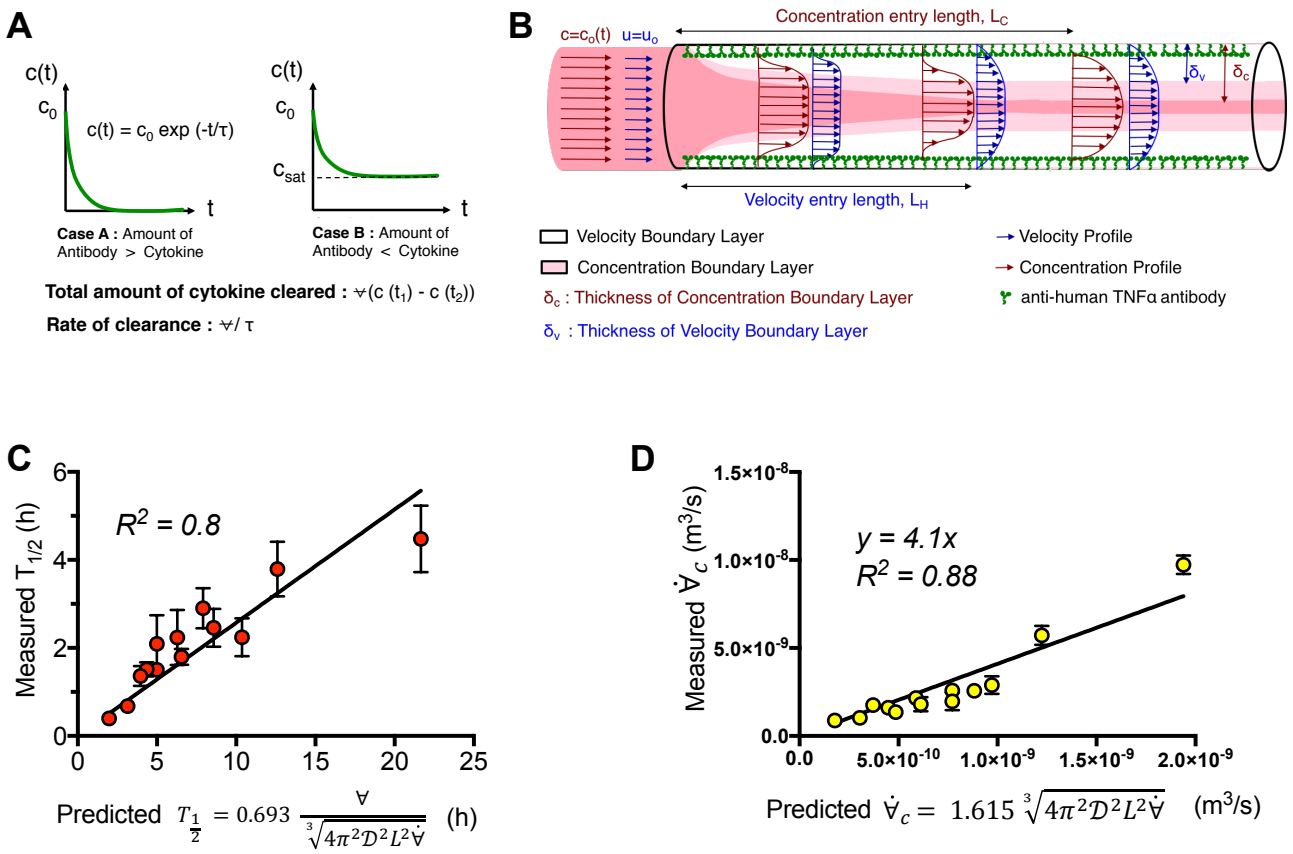

Figure S8. Schematic of fluid flow through AMCs and use of descriptive model to predict cytokine elimination. (A) Two theoretical cytokine elimination curves representing either complete (Case A) or incomplete cytokine elimination (Case B); the latter represents AMC saturation with cytokine (C_{sat}). (B) Schematic of fluid flow through antibody modified conduits (AMCs); thickness of concentration and velocity boundary layers (δ_C and δ_V respectively) vary along the length of AMCs until flow is fully developed (i.e. δ_C and δ_V no longer vary), referred to as concentration (L_C) and hydrodynamic (L_H) entrance lengths. (C) Comparison of theoretical cytokine elimination ($T_{1/2}$) from a predictive model (formulas: $\tau = \frac{\forall}{\sqrt[3]{4\pi^2\mathcal{D}^2L^2\dot{\forall}}}$, $T_{\frac{1}{2}} = 0.693\,\tau = 0.693\,\frac{\forall}{\sqrt[3]{4\pi^2\mathcal{D}^2L^2\dot{\forall}}}$) to measured cytokine elimination (y-axis). C_0, cytokine concentration at time zero. C(t), cytokine concentration at time t. τ, time constant for one phase exponential decay model (same units as x-axis). $\mathcal{D}$, cytokine diffusivity (m^2/sec). L, AMC length (m). $\forall$, reservoir volume (mL). (D) Comparison of theoretical cytokine volumetric clearance from a predictive model (formula: $\dot{\forall}_c = 1.615\sqrt[3]{4\pi^2\mathcal{D}^2L^2\dot{\forall}}$) to measured volumetric clearance (y-axis). $\dot{\forall}_c$, volumetric clearance (m^3/s).

REFERENCES

1. Lee J, Park C, Whitesides G. Solvent Compatibility of Poly(dimethylsiloxane)-Based Microfluidic Devices. *Anal Chem*. 2003;75(23):6544–54.
2. Sui G et al. Solution-Phase Surface Modification in Intact Poly(dimethylsiloxane) Microfluidic Channels. *Analytical Chemistry*. 2006;78(15):5543–5551.
3. Chau K et al. Dependence of the quality of adhesion between poly(dimethylsiloxane) and glass surfaces on the composition of the oxidizing plasma. *Microfluidics and Nanofluidics*. 2011;10(4):907–917.
4. Séguin C, McLachlan JM, Norton PR, Lagugné-Labarthet F. Surface modification of poly (dimethylsiloxane) for microfluidic assay applications. *Applied Surface Science*. 2010;256(8):2524–2531.
5. Nojima Y, Iguchi K, Suzuki Y, Sato A. The pH-Dependent Formation of PEGylated Bovine Lactoferrin by Branched Polyethylene Glycol (PEG)-N-Hydroxysuccinimide (NHS) Active Esters. *Biological and Pharmaceutical Bulletin*. 2009;32(3):523–526.
6. Gandini A. The furan/maleimide Diels–Alder reaction: A versatile click–unclick tool in macromolecular synthesis. *Progress in Polymer Science*. 2013;38(1):1–29.
7. Naik S, Bhattacharjya G, Talukdar B, Patel B. Chemoselective Acylation of Amines in Aqueous Media. *European Journal of Organic Chemistry*. 2004;2004(6):1254–1260.
8. Lee, Blaufox. Blood volume in the rat. *J Nucl Medicine Official Publ Soc Nucl Medicine*. 1985;26(1):72–6.
9. Masel RI. Adsorption II: Adsorption Isotherms. In: Wiley Interscience; 235–244
10. Holzbecher E. Numerical Solutions for the Lévêque Problem of Boundary Layer Mass or Heat Flux. In: Hannover: